

UNCLASSIFIED



Australian Government
Department of Defence
Defence Science and
Technology Organisation

Principles and Application of Magnetic Rubber Testing for Crack Detection in High-Strength Steel Components: II. Residual-Field Inspection

S K Burke, M E Ibrahim and G R Hugo

Maritime Division
Defence Science and Technology Organisation

DSTO-TR-3033

ABSTRACT

Since its introduction in the 1970s, magnetic rubber testing (MRT) has been used successfully to inspect critical high-strength steel aerospace components for surface-breaking fatigue cracks. In the residual-field variant of MRT, inspections are performed following the application and subsequent removal of a magnetic field, relying on the remanent magnetisation of the component to produce crack indications. For certain geometries, residual-field MRT is capable of reliable detection of cracks as small as 0.43 mm (0.017 inch) in surface length. However, for other conditions of specimen geometry and magnet configuration, it was observed that crack indications could be shorter or even absent when using residual-field MRT compared with active-field inspections. This report presents the results of an experimental and theoretical study into the formation of residual-field MRT indications and the rationale for verification of adequate field strength. It is proposed that a combination of inadequate magnetisation, shallow crack depth and the presence of a reversed tangential magnetic field at the surface of the specimen contribute to these observed anomalies in residual-field MRT compared with active-field MRT. The results of a related investigation into active-field MRT are presented in a companion report.

RELEASE LIMITATION

Approved for public release

UNCLASSIFIED

UNCLASSIFIED

Published by

*Maritime Division
Defence Science and Technology Organisation
506 Lorimer St
Fishermans Bend, Victoria 3207 Australia*

*Telephone: (03) 9626 7000
Fax: (03) 9626 7999*

*© Commonwealth of Australia 2015
AR-016-113
December 2014*

APPROVED FOR PUBLIC RELEASE

UNCLASSIFIED

UNCLASSIFIED

Principles and Application of Magnetic Rubber Testing for Crack Detection in High-Strength Steel Components: II. Residual-Field Inspection

Executive Summary

Magnetic rubber testing (MRT) is a sensitive non-destructive testing (NDT) technique used to detect small surface-breaking cracks in critical high-strength steel components.

Historically, the most important application of MRT was the inspection of D6ac high-strength steel components of the F-111 aircraft to ensure their continued structural airworthiness. From 1998 until the withdrawal of the aircraft from service in 2010, the Royal Australian Air Force (RAAF) was sole operator of the F-111. During this period the Defence Science and Technology Organisation (DSTO) undertook a series of studies into the science underpinning the application of MRT, stimulated by concerns about potential unreliability of MRT under some test conditions. The aim of the present report, and the companion report on active-field MRT (DSTO-TR-3032), is to make the results of this work available to the wider NDT community, both to improve the practice of MRT, as well as to stimulate further research into this sensitive inspection technique.

The present work on residual-field MRT was instigated by observations that, for certain conditions of specimen geometry and magnet configuration, crack indications on bare surfaces or at the edges of holes could be shorter or even absent when using residual-field MRT compared with active-field MRT. These observations highlighted that uncertainties remained in the understanding of MRT, despite the use of the technique for over 30 years.

In this report, the technique of residual-field MRT is introduced and the differences between active-field and residual-field inspection are described, drawing on a review of the available literature. Second, the detection of shallow cracks is examined and it is proposed that a combination of inadequate magnetisation, shallow crack depth and the presence of a reversed tangential magnetic field at the surface of the specimen is the likely reason for previously observed anomalies in some residual-field inspections. Third, the basis for verification of adequate magnetisation by measurement of the magnetic field on the surface of the component is considered, with reference to D6ac steel. The possible application of electromagnetic finite element methods for modelling residual-field MRT is then investigated and it is concluded that there are no

UNCLASSIFIED

UNCLASSIFIED

commercially available software packages which can adequately predict the fields produced in practical residual-field MRT. Finally, central-conductor MRT, for which there are fewer uncertainties, is discussed together with suggested design rules for such inspections of D6ac steel.

Drawing the results together, the general conclusion is that active-field MRT is strongly preferred to residual field MRT due to the current lack of design rules for residual-field MRT procedures which would assure the probability of detection (POD) of defects with sufficient confidence. The exception is central-conductor variant of residual-field MRT for which suitable design rules have been established which are supported by empirical POD trials.

UNCLASSIFIED

Authors

S K Burke

Maritime Division



Steve Burke is Group Leader Acoustic Material Systems within Maritime Division and Task Leader for AIR 07/101 Assessment and Control of Aircraft Materials Degradation. His association with electromagnetic nondestructive evaluation research spans several decades. He was awarded a BSc (Hons) from Monash University, and a PhD from Imperial College, London. Steve is a Fellow of the Australian Institute of Physics and a Chartered Physicist.

M E Ibrahim

Maritime Division



Matthew Ibrahim holds a BSc in physics and materials science, and an MSc in theoretical and experimental NDE from Monash University. He has performed NDE research in ultrasonic and electromagnetic NDE at DSTO since 1998, and is currently the Science Team Leader for NDE Research for air platforms under task AIR 07/101.

G R Hugo

Maritime Division



Geoff Hugo is Group Leader Corrosion Science within Maritime Division. He has previously led research programs in advanced electromagnetic and ultrasonic NDE for aircraft applications. Geoff has BSc and BE degrees, and a PhD from Monash University, and is the Australian National Leader for The Technical Cooperation Program Materials Group Technical Panel on Nondestructive Characterisation and Materials State Awareness.

UNCLASSIFIED

This page is intentionally blank

UNCLASSIFIED

Contents

1. INTRODUCTION.....	1
2. BACKGROUND.....	2
2.1 Circular versus longitudinal magnetisation in residual-field MRT	2
2.2 Active-field versus residual-field MRT	3
2.3 Uncertainties in residual-field MRT	6
2.4 Key questions	7
3. LITERATURE REVIEW	7
4. EFFECT OF THE REVERSED TANGENTIAL FIELD IN RESIDUAL-FIELD MRT	11
4.1 Theory	11
4.2 Experiment	16
5. VERIFICATION OF ADEQUATE FIELD STRENGTH	17
6. FINITE-ELEMENT MODELLING.....	19
7. CENTRAL-CONDUCTOR MAGNETIC RUBBER TESTING.....	20
8. FUTURE WORK.....	23
9. CONCLUSIONS.....	23
APPENDIX A: RESIDUAL MAGNETISATION.....	29
APPENDIX B: CENTRAL-CONDUCTOR FIELD CALCULATOR	32

Abbreviations

2-D	Two dimensional
3-D	Three dimensional
ADF	Australian Defence Force
CCMRT	Central conductor MRT
CGS	Centimetre Gram Second electromagnetic measurement units
DC	Direct current
DGTA-ADF	Directorate General Technical Airworthiness – ADF
DSTO	Defence Science and Technology Organisation
D6ac	Denotes a grade of high strength steel
FEM	Finite element modelling (for calculating magnetic fields)
MFI	Magnetic flux indicator
MFL	Magnetic flux leakage (inspection technique)
MPI	Magnetic particle inspection
MRT	Magnetic rubber testing
NDE	Non-destructive evaluation
NDT	Non-destructive testing
NDT&CT	Non-destructive Testing & Composite Technology (within DGTA-ADF)
POD	Probability of detection (of a crack)
RAAF	Royal Australian Air Force
SI	International System of Units

Symbols

a_{NDI}	Length of the smallest crack that can be reliably detected
b	Crack depth
B	Magnetic Induction, Magnetic Flux Density
B	Magnitude of Magnetic Induction = $ \mathbf{B} $
B_r	Remanent Magnetic Induction (Remanence)
F_{mag}	Magnetic force on a spherical particle
H	Magnetic Field Strength, Magnetising Force

H	Magnitude of Magnetic Field Strength = $ H $
H_c	Coercive field
H_{crack}	Leakage field due to a crack
H_n	Component of H normal (perpendicular) to the surface of a material
H_{max}	Maximum excursions of H for a minor hysteresis loop or, for residual-field inspection, the largest value of H applied to the specimen before it is removed to leave the specimen in a remanent magnetic state.
H_t	Component of H tangent (parallel) to the surface of a material
k	Length to maximum diameter ratio of an ellipsoid
M	Magnetisation
M_0	Specimen magnetisation
N_d	Demagnetisation factor
σ_s	Magnetic pole density
μ_0	Permeability of free space
ν	Permeance coefficient
V	Particle volume

UNCLASSIFIED

DSTO-TR-3033

This page is intentionally blank

UNCLASSIFIED

1. Introduction

Since its introduction in the 1970s, magnetic rubber testing (MRT) has been used successfully to inspect critical high-strength steel aerospace components for small surface-breaking fatigue cracks.

Historically, the most important application of MRT was the inspection of D6ac high-strength steel components of the F-111 aircraft to ensure their continued structural airworthiness. From 1998 until the withdrawal of the aircraft from service in 2010, the Royal Australian Air Force was sole operator of the F-111. During this period the Defence Science and Technology Organisation (DSTO) undertook a series of studies into the science underpinning the application of MRT, stimulated by concerns about potential unreliability of MRT under some test conditions. The results of this program were progressively communicated to the RAAF airworthiness authority (Directorate General of Technical Airworthiness, DGTA) and the F-111 maintenance community via an ongoing series of DSTO technical reports, as well as numerous DSTO client reports, internal minutes and memoranda throughout the period 2005 to 2009.

The aim of the present report, and the companion report on active-field MRT [1], is to make the results of this work available to the wider NDT community, both to improve the practice of MRT, as well as to stimulate further research into this sensitive inspection technique.

In the residual-field variant of MRT, inspections are performed following the application and subsequent removal of a magnetic field, relying on the remanent magnetisation of the component to produce crack indications. Probability of detection (POD) studies have demonstrated that for certain geometries, residual-field MRT is capable of reliable detection of cracks as small as 0.43 mm (0.017 inch) in surface length [2].

The present work examines the fundamentals of residual-field MRT. It was initiated by the observation that, for certain conditions of specimen geometry and magnet configuration, crack indications on bare surfaces or at the edges of holes could be shorter or even absent when using residual-field MRT compared with active-field inspections. These observations indicated that uncertainties remained in the understanding of MRT, despite the widespread use of the technique for over 30 years.

The report is structured around the following key questions:

- What is already known in literature on the differences between active- and residual-field MRT for defect detection?
- What is the mechanism responsible the appearance of weakened indications or white bands in residual-field MRT with longitudinal magnetisation?
- How is adequate residual magnetisation achieved in residual-field MRT and how is it verified?

- Is electromagnetic finite-element modelling (FEM) sufficiently mature to assist in the design of practical MRT inspections?

and, finally,

- Can the design rules and practice of central-conductor MRT (CCMRT) be further improved?

We adopt the CGS system of electromagnetic units, Gauss (G) for magnetic induction B , and Oersted (Oe) for magnetic field strength H to be consistent with RAAF practice. Conversion to the corresponding SI units (Tesla and A/m) is as follows: 1 Oe = 79.58 A/m and 1 G = 0.1 mT.

2. Background

For both active- and residual-field MRT, magnetic particles suspended in liquid silicone rubber are poured onto the inspection site and the rubber is allowed to cure. The presence of a surface-breaking crack will become evident through the attraction of magnetic particles in the liquid rubber to the mouth of the crack, due to leakage of the magnetic flux out of the component near the crack. The increasing viscosity of the curing rubber eventually traps the particles in location, allowing a permanent record of the crack indication to be formed on the surface. In residual-field MRT, the component is magnetised and the source of external magnetism is then removed before the rubber is applied to the component. The rubber thus cures in the absence of any externally applied magnetic field and the technique relies on leakage of the remanent magnetic flux remaining after magnetisation to form a crack indication.

The use of residual-field MRT is described in the original 1975 General Dynamics patent for magnetic rubber testing and has since been used extensively [3]. The main benefits of the technique compared to active-field MRT are ease of access and convenience, as the magnetising equipment is removed from the region of interest prior to pouring the magnetic rubber. An additional benefit is that magnetic rubber casts obtained using the residual-field technique are frequently clearer and exhibit less magnetic noise than those prepared in active-field inspections.

2.1 Circular versus longitudinal magnetisation in residual-field MRT

It is important to distinguish between two broad magnetisation geometries which arise in residual-field MRT, circular magnetisation and longitudinal magnetisation, shown schematically in Figure 1. For circular (or circumferential) magnetisation, the specimen is magnetised in such a way that the applied magnetic field forms closed loops around the specimen and there are no magnetic north or south poles created on the specimen surface, Figure 1(a). On removal of the applied field, a circumferential residual magnetisation remains and, due to the absence of magnetic poles, the field outside the specimen is zero, Figure 1(b). Circular magnetisation can be achieved by injection of a DC current through the specimen itself, Figure 1(a), through the use of a central-conductor, as in tube or hole inspection, or for ring-shaped specimens by a toroidal cable-wrap [4].

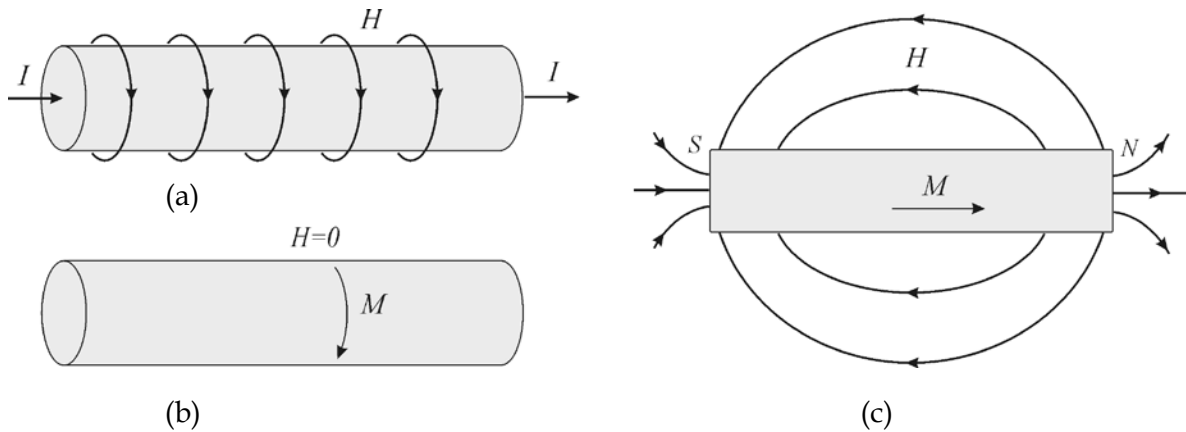


Figure 1 Magnetisation in residual-field MRT (schematic): (a) and (b) circular magnetisation, (c) longitudinal magnetisation.

For longitudinal specimen magnetisation, the magnetic field is applied parallel to the long axis of the part using either a cable-wrap solenoid, permanent magnet or a DC electromagnet. In this configuration, the applied magnetic field enters or leaves at least some portion of the specimen surface, leading to the creation of magnetic poles which remain on removal of the applied field, Figure 1(c). The presence of such magnetic poles is the important feature of longitudinal magnetisation in residual-field MRT.

2.2 Active-field versus residual-field MRT

The fundamental difference between active- and residual-field MRT can be illustrated using the B - H curve for D6ac steel shown in Figure 2. For active-field MRT, the magnetic flux density B in the test specimen follows the normal magnetic induction curve (a) to an operating point in the 1st quadrant of the B - H plane defined by the applied magnetic field strength H . For residual-field MRT, the component is initially magnetised along the normal curve (a) to a point in the 1st quadrant defined by the maximum applied field H_{max} , but on removal of the applied field the component behaves like a permanent magnet for which the operating point during the application and cure of the rubber lies on the hysteresis curve (b), in the 2nd quadrant.

As active-field MRT is conducted in the 1st quadrant of the material B - H curve, the magnetisation M , magnetic induction B and magnetic field strength H are all positive within the material. Residual-field MRT is confined to the 2nd quadrant, where M and B are positive but H is negative or zero. The case where $H = 0$ corresponds to circular magnetisation, as in CCMRT. The case where H is negative occurs for longitudinal magnetisation, due to the presence of a demagnetisation field arising from magnetic poles on the surface of the specimen, Figure 1(c) [5-7]. As a result, for residual-field MRT with longitudinal magnetisation, the tangential component of the magnetic field strength (H_t) at the surface of the specimen is opposite in sign (antiparallel) to the specimen magnetisation. This 'reversed tangential field' can be highly significant in the formation of indications for shallow cracks, and is discussed in more detail in Section 4.

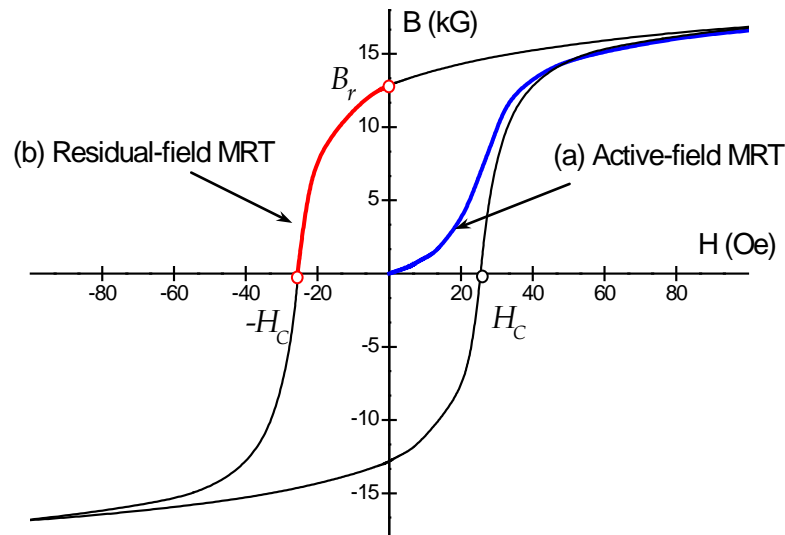


Figure 2 Regions of the B - H curve for D6ac steel corresponding to (a) active-field MRT (blue curve) and (b) residual-field MRT (red curve). The coercive field H_c and remanent magnetic flux density B_r are shown.

The relationship between B , M and H is depicted schematically for the case of an ellipsoidal test specimen* for active-field MRT (1st quadrant of B - H) in Figure 3 and residual-field MRT (2nd quadrant of B - H) in Figure 4.

The second major difference between active- and residual-field MRT is due to the different role that the magnetic history of the specimen plays in determining the final magnetic state. Assuming an initially demagnetised test specimen,

- In active-field MRT, B and H are related by the normal induction curve (Figure 2 curve a), so that for a well-designed MRT inspection the magnetic state of the specimen can be uniquely determined by measurement of the external value of H_t alone (using the continuity of H_t across the air-steel interface).
- In residual-field MRT, the relationship between B and H is characterised by a series of hysteresis loops, each loop corresponding to the past magnetic history of the specimen. Unlike active-field MRT, the magnetic state of the specimen cannot be uniquely identified by measuring the external value of H but also requires knowledge of the magnetic history of the specimen, for example, the largest value of field used to magnetise the specimen [5].

* An ellipsoidal specimen is a particularly useful illustrative case because, unlike other shapes, an ellipsoid can sustain a uniform magnetisation within the volume of the specimen.

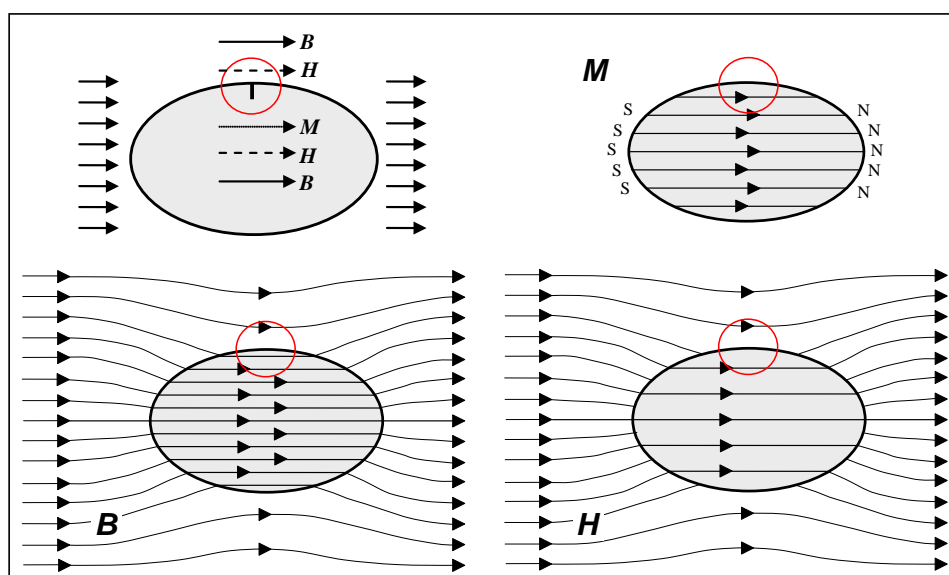


Figure 3 Relationship between M , B and H for active-field MRT: ellipsoidal specimen in a uniform applied field. The top-left figure shows the specimen geometry and the fields, and the remaining three figures plot the field lines for each of M , B and H . The region of interest (red circle) shows that M , B and H are parallel for active-field MRT. The field due to the defect is not shown.

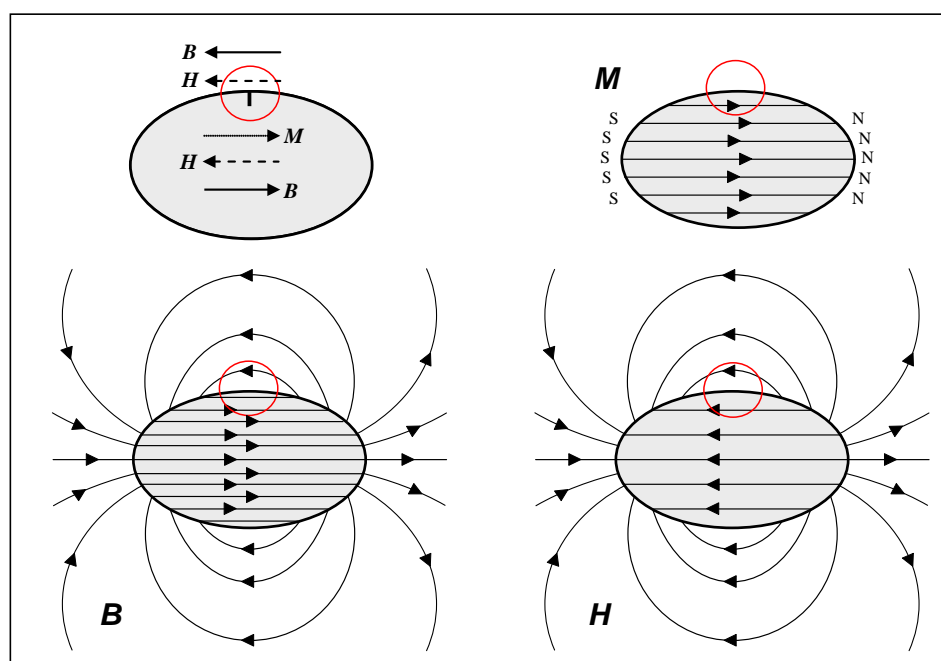


Figure 4 Relationship between M , B and H for residual-field MRT: uniformly magnetised specimen in zero field. The top-left figure shows the general geometry of specimen and fields, and the remaining three figures plot the field lines for each of M , B and H . The region of interest (red circle) shows that the direction of H is opposite to that of M for residual-field MRT. The field due to the defect is not shown.

2.3 Uncertainties in residual-field MRT

Although residual-field MRT has been in use for over 30 years, it was only during the last decade that a number of uncertainties in our understanding of the technique became apparent. These uncertainties were highlighted through a series of investigations undertaken by the RAAF Non-destructive Testing & Composite Technology (NDT&CT) and subsequently at DSTO. In particular, it was observed that the length of some crack indications could be significantly shorter, or even absent under certain conditions of specimen geometry and magnet configuration when using residual-field compared with active-field MRT.

Figure 5(a) illustrates an optimal residual-field inspection result. Here, the crack indications are slightly longer and more distinct than those for corresponding active-field inspection. However, for the residual-field inspection shown in Figure 5(b), the crack indication is either significantly shorter or absent altogether. In some cases, it was observed that the normally black crack indication was replaced by a weak white band at the crack location.

The anomalies were uncorrelated with the measured tangential component of the residual field at the surface of the specimen.

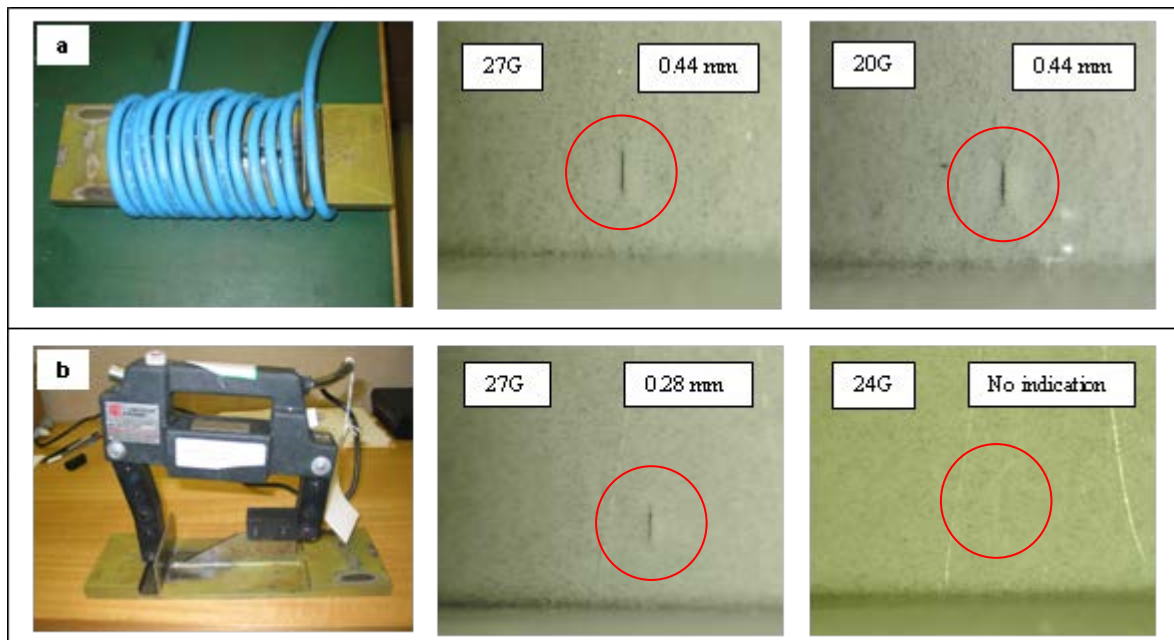


Figure 5 Variability in residual-field MRT indications for a fatigue crack in a D6ac steel test piece. The initial magnetisation was applied using (a) a pulsed DC cable-wrap solenoid and (b) a DC electromagnet. In the final image, the crack indication is absent apart from a faint white band at the crack position. The values of the tangential component of the residual magnetic field at the crack location are indicated. The nominal crack length obtained from active-field MRT is 0.36 mm (0.014 inch). Images courtesy NDT&CT.

While a number of unrelated sources of potential reliability had also been identified for CCMRT, it became clear as the DSTO studies progressed that the observed anomalies in residual-field MRT highlighted in this section were specific to longitudinal magnetisation geometries, such as those shown in Figure 5.

2.4 Key questions

With this background, the DSTO investigations into residual-field MRT centred on the following key questions:

- What is already known in literature on the differences between active- and residual-field MRT for defect detection?
- What is the mechanism responsible for the appearance of weakened indications or white bands in residual-field MRT with longitudinal magnetisation?
- How is adequate residual magnetisation achieved in residual-field MRT and how is it verified?
- Is electromagnetic finite-element modelling sufficiently mature to assist in the design of practical MRT inspections?

and, for completeness,

- Can the design rules and practice of CCMRT be further improved?

These questions are addressed in the remainder of this report, commencing with a literature search into the effects on defect detectability arising from the differences in active- compared with residual-field MRT.

3. Literature Review

Apart from a reference to the use of residual fields in the original MRT patents* [3, 8] and in practical inspection procedures, no significant information relating specifically to residual-field MRT could be found in the available scientific and technical literature. The authors therefore concentrated on results for the related magnetic inspection techniques of magnetic flux leakage (MFL) and magnetic particle inspection (MPI). The review concentrated on literature for flux leakage from narrow slots and crack-like defects, rather than volumetric defects such as gouges or flat-bottom holes which are more relevant to oil-pipeline inspection [9].

Several authors have investigated the differences between active- and residual-field techniques for the idealised two-dimensional (2-D) geometry where bars, rods and tubes containing a longitudinal slot are magnetised using a circumferential field produced by

* The original patent describes a residual inspection technique as follows: 'The proper field is conveniently introduced into D6ac steel [...] by energising a DC electromagnet at a high setting for a short time [...] then turning it off. The resulting magnetic field remains at about 30 Gauss.'

either an injected current (bars and rods) or a central conductor (tubes) [10-16]. In this configuration, in which the test piece provides a closed loop magnetic circuit in the circumferential direction, specimen demagnetisation effects are negligible and the magnetic field H external to the magnetised component for the residual-field case will be approximately zero in the absence of a defect, due to the circular magnetisation within the material, as discussed in Section 2.

For narrow* slots, the results can be summarised as follows:

- Residual leakage fields for any given magnetisation conditions are significantly smaller than active leakage fields,
- For large applied fields H_{max} , the residual leakage fields increase with increasing slot depth for a given slot width and decrease with increasing slot width for a given slot depth [11, 13, 15, 17],
- As noted for residual leakage field, for active-field leakage fields all reports show that the leakage field increases with slot depth. The literature however contains contradictory reports on the variation of active leakage fields with slot width. In some cases the leakage field is found to increase with increasing slot width [12, 16] (for very narrow slots) and in other cases the field decreases with increasing slot width [11, 15, 17, 18] (for wider slots). One possible explanation for these inconsistencies is that the leakage field for a closed slot is initially zero, increases rapidly with slot depth, reaches a peak and then decreases. There is some limited evidence for such behaviour in the results of a MSc thesis by Heath [15]. In this way, narrow slots will show an increase in leakage field with slot width and wider slots will show a decrease†. This explanation is then consistent with observations made using fatigue cracks [19, 20] for which there is a rapid increase in leakage field as the crack opening displacement is increased. It is not clear whether similar behaviour is expected for residual fields.
- There are subtle differences in the spatial distribution of residual leakage fields compared with active leakage fields due to a slot.
 - Stanley [12] observed that the active leakage field gradients at the surface increase with increasing slot width for a given slot depth whereas the residual-field gradients decrease with increasing slot width for the same slots. This conclusion is based on both photomicrographs of MPI indications for slots of increasing width as well as quantitative data using pickup coils for slots of varying widths in longitudinal fields.
 - The variation of the leakage field with depth within the slot is different for active and residual fields. According to Förster [17], for active fields the field strength inside the slot decreases towards the bottom of the slot, whereas for residual fields the field strength increases towards the bottom of the slot.

* Only slots for which width/depth ≤ 1 were considered

† The situation is further complicated by the effect of probe liftoff (distance from the surface) so that Förster [17] reports that for large lift-off, the tangential leakage fields are independent of slot width.

- For three-dimensional (3-D) slots (i.e. slots with finite length as opposed to long '2-D' slots with only depth and width dimensions), Lord and Srinivasan [21] report a pronounced difference in the shape of the residual and active leakage field profiles near the ends of the slot. The residual-field leakage case shows a distinct concentration in the peak-to-peak flux density near the ends of the slot. This concentration is absent in the active-field flux leakage case.
- There are major differences in the behaviour of active compared with residual leakage fields as a function of the strength of the applied magnetic excitation. The magnitude of the active leakage field increases monotonically as the applied magnetic field is increased, with evidence of a threshold at lower fields [12, 14]. The threshold is located in the vicinity of the coercive field H_c . The variation of the residual leakage field with the maximum applied field H_{max} is more complicated and is discussed below.

Heath [14, 15] investigated the behaviour of active and residual leakage fields from slots in rectangular AISI 1020 steel bars using an approximately 2-D configuration with the magnetic field generated using DC current injection. The results are summarised in Figure 6 which is adapted from Heath's publication. For active-field MFL, the leakage field increased linearly with applied current above a threshold current. For residual-field MFL however, the leakage field was found to cross zero and change polarity below a certain excitation current level [14].

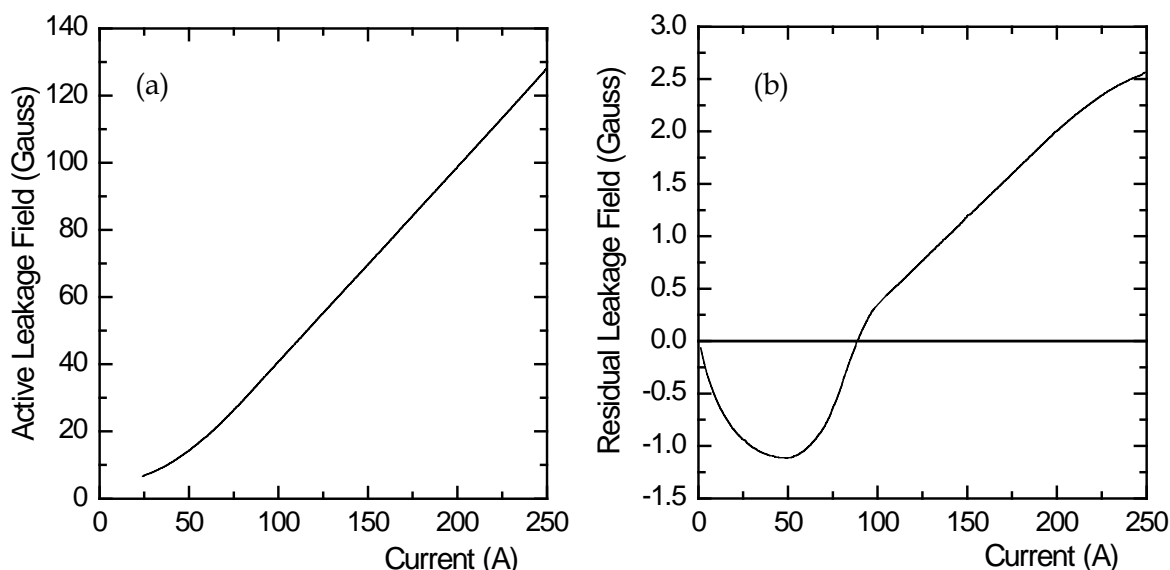


Figure 6 (a) Active and (b) residual leakage fields at the surface due to a slot in AISI 1020 steel as a function of injected magnetising current, showing the polarity reversal for the residual defect field [14]. For the active-field case, the current is maintained during the measurement and then set to zero for the corresponding residual-field measurement. Field values are the peak-to-peak values of the perpendicular component of the defect leakage field measured as a function of position across the slot. This figure is adapted from the original work by Heath [14].

This reversal in polarity had also been observed by Förster [17] who concluded that the field reversal was only observed for values of the previously applied field H_{max} typically less than H_c . Förster [17] attributed the reversal to the presence of a residual field 'diverted flux dipole' (volume magnetic charges) at the crack tip. This field reversal was already known to Soviet authors in 1965 [22]. Unfortunately, apart from the initial study by Heath [15], no systematic investigations of the field reversal phenomenon as a function of defect dimensions or specimen magnetic properties are evident in the literature.

The theory of residual-field leakage from surface-breaking defects is not as well established as the theory for active fields [1]. Apart from the semi-quantitative description presented by Förster [17, 18], the most useful theory is due to Zagidulin [22, 23] who developed a simplified analytical model to predict the remanent flux leakage from a 2-D defect inside a ferromagnetic half-space. The model, which takes into account non-linearity and magnetic hysteresis, represents the leakage field using a residual surface charge density on the faces of the defect and, similar to Förster [17, 18], an equivalent magnetic flux dipole to account for volume magnetic charges. This model successfully accounts for the defect field polarity reversal and also predicts a reduction in the residual leakage field with increasing defect width. The predictions of the model are also in reasonable quantitative agreement with Förster's earlier experiments [17, 18].

In view of the greater complexity of residual-field compared with active-field problems, there is great potential value to be gained from the use of numerical modelling techniques such as electromagnetic FEM. For example, Heath [15] was able to examine the distribution of residual magnetic flux in the vicinity of a rectangular slot in order to explain the defect field polarity reversal phenomenon shown in Figure 6(b). However, the state of the art for residual-field modelling applied to NDE appears to be restricted to 2-D geometries.

While studies of artificial defects such as electro-discharge machined slots provide useful information, flux leakage from fatigue cracks is more complicated than for such artificial defects. For fatigue cracks, additional flux contributions, thought to be associated with plastic deformation, are reported near the edges of the crack for active-field excitation [20]. These 'satellite peaks' in the magnetic flux are opposite in polarity to the principal component of the leakage flux which exhibits the form expected for a narrow slot. The behaviour of these satellite peaks for residual-field excitation is not known.

Crack closure effects are also important so, for example, the active-field magnetic leakage flux increases dramatically when the crack opening displacement is increased through the application of a remote tensile stress [20], as illustrated by the work of Sponder *et al.* [19] for fatigue cracks in D6ac. A similar phenomenon was found in other experiments conducted by DSTO which demonstrated that the length of MRT indications increased slightly if inspections were performed under tensile load [24, 25]. The effect of crack closure on residual-field leakage flux is not well known.

Stanley [12] asserts that both cracks and narrow flaws give stronger defect indications in residual-field MPI than in active-field MPI. This conclusion is based on observations for a crack as well as for a series of narrow machined slots, and is supported by the residual-

field MRT indication shown in Figure 5(a), which is longer than the equivalent active-field MRT indication. However, this is clearly not the case for the residual-field MRT casts reproduced in Figure 5(b), where the crack indications are shorter or absent under residual-field conditions compared with active-field MRT. It is therefore unlikely that any general statements can be made on crack detectability for residual- compared with active-field MRT or MPI without tight specification of the test parameters, specimen geometry, material magnetic properties and field configuration.

In summary, a review of the literature shows several important differences in the behaviour of residual leakage fields from surface-breaking defects compared with active leakage fields. Residual leakage fields are smaller in magnitude, display a different spatial distribution within the defect and can exhibit a field-polarity reversal if the initially applied field is small. As was found for active-field MRT, the literature reveals a broad but incomplete theoretical background for residual-field MRT. There are, at present, no validated models which could be used directly to assist in understanding the performance of practical residual-field MRT.

The literature search did not reveal any discussion on possible mechanisms for the appearance of weakened indications or white bands in residual-field MRT with longitudinal magnetisation (Section 2.3). A simple model was therefore developed to examine the likely mechanism and is presented in the next section.

4. Effect of the Reversed Tangential Field in Residual-Field MRT

A simplified 2-D model was developed to explore the implications of a reversed tangential magnetic field on the formation of crack indications in residual-field MRT. The theory is an extension of the model used previously to examine the effect of the normal component of magnetic field in active-field MRT [1].

4.1 Theory

The magnetic fields in the vicinity of a 2-D crack are shown schematically in Figure 7 and consist of the leakage field due to the crack H_{crack} , together with the local tangential (H_t) and normal (H_n) components arising from the remote field due to magnetisation of the specimen. According to this construction,

$$\mathbf{H} = \hat{\mathbf{y}} H_n + \hat{\mathbf{x}} H_t + \mathbf{H}_{crack} . \quad (1)$$

The magnetic force on a spherical magnetic particle is given the expression [1]

$$\mathbf{F}_{mag} = \mu_0 V \nabla (\mathbf{H} \cdot \mathbf{H}) \quad (2)$$

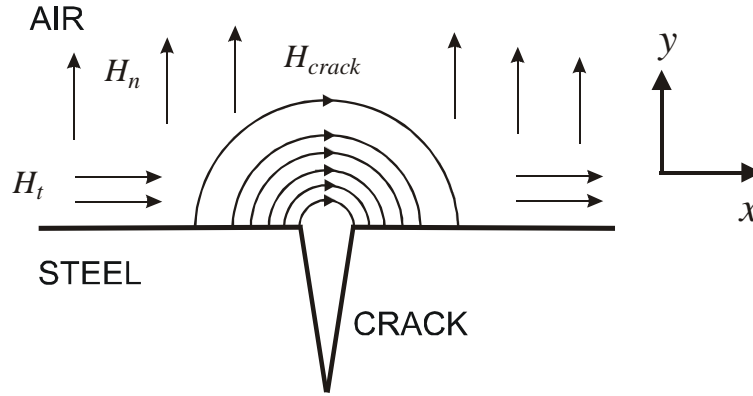


Figure 7 Simplified diagram showing the behaviour of magnetic fields near a 2-D crack.

where V is the particle volume and the relative permeability of the particle is assumed to be large. Substituting Eq. (1) into Eq. (2), the magnetic force on a particle can be written

$$\mathbf{F}_{mag} = \mu_0 V \nabla \left[\left(H_t + H_{crack}^x \right)^2 + \left(H_n + H_{crack}^y \right)^2 \right], \quad (3)$$

where H_{crack}^x and H_{crack}^y denote the x and y components of the leakage field from the crack. Assuming for simplicity that the remote normal component of field H_n is zero, the x and y components of the magnetic force on the particle can be obtained from Eq. (3):

$$\begin{aligned} F^x &= 2\mu_0 V \left[\left(H_t + H_{crack}^x \right) \frac{\partial H_{crack}^x}{\partial x} + H_{crack}^y \frac{\partial H_{crack}^y}{\partial x} \right], \\ F^y &= 2\mu_0 V \left[\left(H_t + H_{crack}^x \right) \frac{\partial H_{crack}^y}{\partial x} - H_{crack}^y \frac{\partial H_{crack}^x}{\partial x} \right]. \end{aligned} \quad (4)$$

Thus, in the presence of a reversed tangential field ($H_t < 0$), it is possible for the factor $(H_t + H_{crack})$ which enters the expression (4) for the magnetic force to become negative, leading to a region of repulsive magnetic force $F^y > 0$ above the crack. In the extreme case, if the crack field H_{crack} is weak enough, due to either shallow crack depth or inadequate magnetisation, the repulsive force is predominant and may drive the magnetic particles away from the crack, leading to a white band instead of the normal dark crack indication.

Computations illustrating the effect of a reversed tangential field on the forces above a 2-D crack in residual-field MRT were performed assuming that the leakage field due to the crack is given by the expressions derived by Edwards and Palmer [26]

$$\begin{aligned} H_{crack}^x &= \frac{\sigma_s}{2\pi} \left(\arctan \left[\frac{b(x+a)}{(x+a)^2 + y(y+b)} \right] - \arctan \left[\frac{b(x-a)}{(x-a)^2 + y(y+b)} \right] \right), \\ H_{crack}^y &= \frac{\sigma_s}{4\pi} \log \left[\left(\frac{(x+a)^2 + (y+b)^2}{(x-a)^2 + (y+b)^2} \right) \left(\frac{(x-a)^2 + y^2}{(x+a)^2 + y^2} \right) \right], \end{aligned} \quad (5)$$

where b is the crack depth, $2a$ is the crack opening width and σ_s is the magnetic pole density. For residual-field MRT, provided the crack is narrow ($b/a \ll 1$) it can be assumed as a first approximation that [1, 26]

$$\sigma_s = 2M_0, \quad (6)$$

where M_0 is the specimen magnetisation.

The calculations were carried out using the same crack parameters ($b=0.25$ mm, $a=5$ μ m) as in DSTO-TR-3032 [1], but using two different states of residual magnetisation deduced from the 2nd quadrant B - H curves for D6ac steel, Appendix A. In both cases $H_t = -20$ Oe and $H_n = 0$. In the first example, the B - H curve corresponding to $H_{max} = 250$ Oe is used and the resulting magnetisation $M_0 = 7500$ Oe is adequate. In the second example, the B - H curve for $H_{max} = 30$ Oe is used, producing a potentially inadequate magnetisation $M_0 = 500$ Oe.

The results are depicted in Figure 8 which shows the force acting on a magnetic particle as a function of its position relative to the crack mouth at $x = 0, y = 0$.

The forces shown in Figure 8 demonstrate that a reversed tangential field produces a region of magnetic particle repulsion above a certain height y_r over the crack, and a region of particle attraction below this height

$$F_0^y(0, y) > 0 \quad \text{for} \quad y > y_r. \quad (7)$$

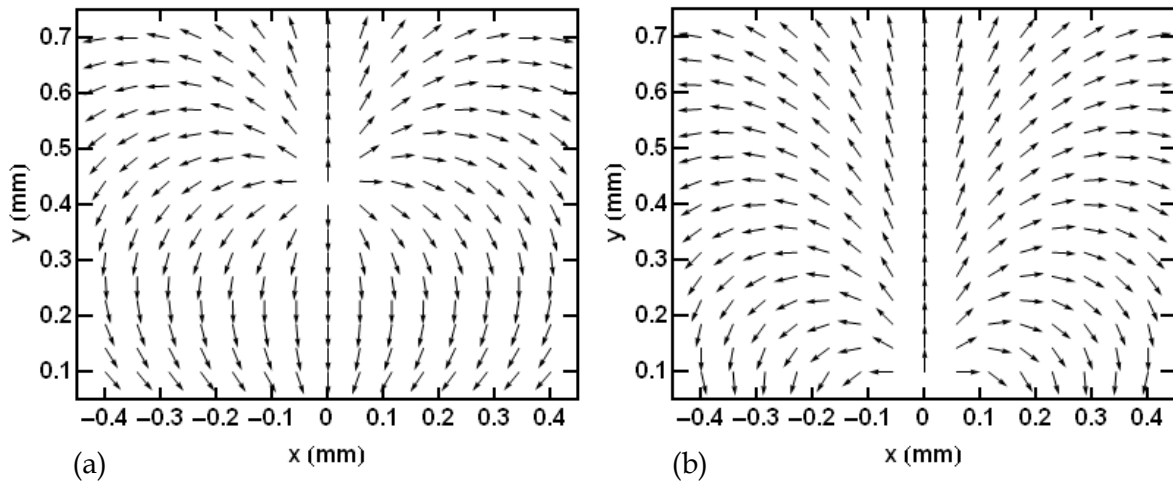


Figure 8 Effect of a reversed tangential component of magnetic field on the forces acting on a magnetic particle above a 2-D crack. (a) $H_t = -20$ Oe, $M_0 = 7500$ Oe, (b) $H_t = -20$ Oe, $M_0 = 500$ Oe. A leakage field from the crack of the form given by Eq. (5) is assumed. The crack mouth is at $(0,0)$. The length of the arrows is related to the magnitude of the force via a logarithmic scale.

The proximity of the region of repulsive force to the surface of the specimen depends on the strength of the magnetisation, the crack opening and the depth of the crack. Using the Edwards-Palmer [26] model for the leakage field Eq. (5), together with Eq. (4), it can be shown that there are two cases, depending on the size of the tangential field. In the first case,

$$\text{if } H_t < 0 \quad \& \quad |H_t| > \alpha M_0 \quad \text{then} \quad y_r = 0, \quad (8)$$

where $\alpha = (2/\pi) \arctan(b/a)$ and the force is always repulsive at all heights above the crack. In the second case,

$$\text{if } H_t < 0 \quad \& \quad |H_t| < \alpha M_0 \quad \text{then} \quad y_r = -\frac{b}{2} + \frac{1}{2} \left(b^2 - 4a^2 + 4ab \cot \left[\frac{\pi |H_t|}{2M_0} \right] \right)^{1/2}, \quad (9)$$

and the region of repulsive force depends explicitly on the crack dimensions and the relative size of the reversed tangential field compared with the magnetisation.

It follows from Equations (8 - 9) that there is always a region of repulsive force above the crack if there is a reversed tangential field ($H_t < 0$). Furthermore, the proximity of the region of reversed force depends on the ratio H_t/M_0 and for a given crack geometry will become closer to the surface if either the magnetisation is inadequate (low) or the reversed tangential field is large. According to Eq. (8), if $H_t < -\alpha M_0$ the forces on the magnetic particles will be repulsive at all heights above the crack mouth, leading to a white band at the crack location in place of a normal crack indication, as has been observed in practice.

Similar conclusions can be drawn if the leakage field takes the simpler form [27]

$$H_{crack}^x = \frac{2\lambda b}{\pi} \frac{y}{x^2 + y^2}, \quad H_{crack}^y = -\frac{2\lambda b}{\pi} \frac{x}{x^2 + y^2}, \quad (10)$$

where λ is a scaling factor dependent on the applied field strength and magnetisation.

It can also be shown in this case that there is a region where the magnetic force is repulsive above the crack in the presence of a reversed tangential field. If $H_t < 0$ then

$$y_r = \frac{2\lambda b}{\pi |H_t|}. \quad (11)$$

Similar to Equations (8 - 9), Eq. (11) shows that the proximity of the region of repulsive force to the surface of the specimen depends on the strength of the leakage field compared with the reversed tangential field. Furthermore, the proximity of the region of repulsive force is closer to the surface for shallow cracks than for deeper cracks.

A series of highly simplified 2-D computer simulations was carried out to examine the effect of a reversed tangential field on residual-field MRT indications using the method described previously [1]. The results are shown in Figure 9 for (a) an unmagnetised specimen $\lambda = 0$, (b) zero tangential field $H_t = 0$, and (c) a reversed tangential field $H_t = -1$. In cases (b) and (c), it was assumed for illustrative purposes that $\lambda = 1$, $b = 0.5$ mm and $H_n = 0$. The simulated indications confirm that it is possible under certain conditions for a negative (reversed) tangential field to produce a faint white band at the crack position.

Note that the theory presented in this section assumes that the polarity of the leakage field H_{crack} shown in Figure 7 is the same as it would be for active-field MRT, i.e. the applied magnetic field H_{max} is assumed to have been sufficiently large that the residual leakage field is not 'reversed' (see Section 3 and Figure 6).

Drawing together these model results, the presence of a reversed tangential field at the specimen surface coupled with a weak leakage field due to inadequate magnetisation and a shallow crack depth is the likely reason for the observed reduction in length of some residual-field MRT crack indications (Figure 5b). The absence of a crack indication and the presence of a faint white band can also be attributed to these factors. To the authors' knowledge, these observations have not been explained previously and follow from an analysis of the forces acting on a magnetic particle.

Several factors in the formation of residual-field MRT indications for shallow cracks are not well understood. The role of regions of reversed leakage field due to plastic deformation near the crack tip has not been considered, nor has the potential effect of the field reversal for low H_{max} (c.f. Section 3). The influence of the normal component of residual field has also not been fully investigated. Finally, the simplified model developed here treats the fields from the crack using a 2-D approximation and ignores the actual 3-D character of the leakage fields from a finite-length defect. Further research would be required to clarify these and other complexities.

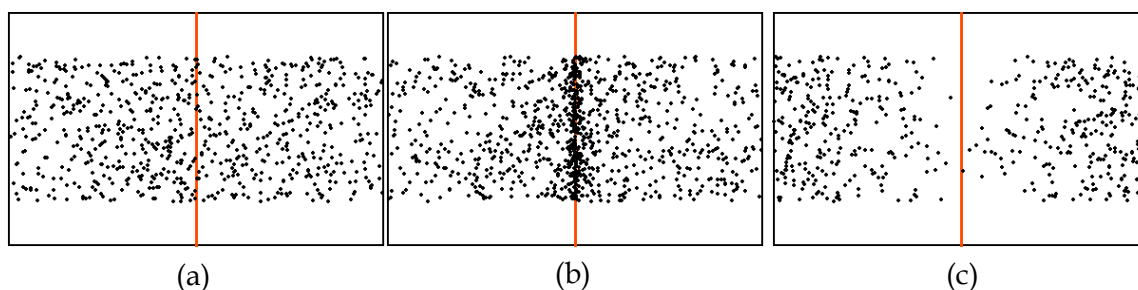


Figure 9 Effect of reversed tangential field. MRT indications obtained from 2-D computer simulations for (a) an unmagnetised specimen, (b) zero tangential field resulting in a strong indication, and (c) reversed (negative) tangential field $H_t = -1$ resulting in white banding. The crack location is at the red line. The magnetic field is expressed in scaled arbitrary units.

4.2 Experiment

The theory developed in Section 4.1 can be used to explain a further anomaly observed by NDT&CT – a distinct white band forming part of a particular residual-field MRT crack indication. The anomaly was noted during a series of trial inspections performed on a D6ac steel bolthole coupon prepared for earlier DSTO POD studies [24, 25]. The test specimen contained a corner crack with a length of 0.68 mm (0.027 inch) on the surface and 0.84 mm (0.033 inch) in the bore.

The two trial crack indications obtained by NDT&CT using different residual-field MRT conditions are shown in Figure 10. The first image, Figure 10(a), was obtained using conventional residual-field MRT with a magnetising yoke. The second image, Figure 10(b), was obtained in the same way but with the test coupon clamped on top of a stack of steel plates so that a large volume of metal was magnetised. The measured tangential component of residual field in the region of interest was 18 Oe in both cases. As expected, the first image shows a distinct black crack indication 0.52 mm long, slightly shorter than the actual crack length in this case. However, in the second image, Figure 10(b), rather than a single distinct indication, as in Figure 10(a), a faint black indication 0.23 mm in length can be seen extending from the bolthole together with a white band extending from the tip of the black indication to the end of the crack. The combined length of the indication and white band is 0.66 mm, equal to the length of the crack.

The white band shown in Figure 10(b) can be explained by the variation of the strength of the leakage field compared to the reversed tangent field along the length of the crack. The faint indication occurs near the edge of the bolthole, where the crack is deepest and the leakage field is largest. The white band occurs where the crack is shallow and the leakage field is relatively weaker compared to the reverse tangential field immediately above the crack. The transition point between the normal (but weak) dark indication and the white band depends on the strength of the leakage field compared with the reversed tangential field and the depth profile of the crack.

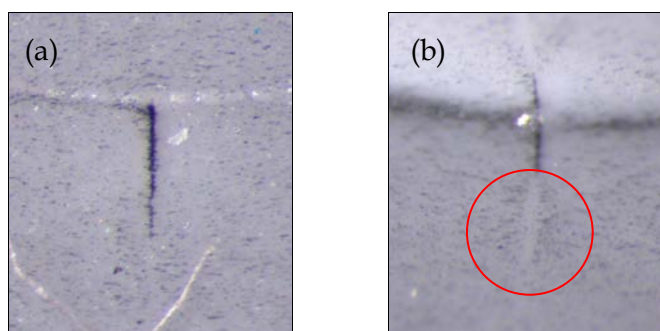


Figure 10 Residual-field MRT indications (surface) for a quadrant crack of surface length 0.68 mm (0.027 inch) in D6ac steel. In case (a) a strong crack indication is present, whereas in case (b) the indication shows the presence of a significant white band at the end of the crack. In both cases the measured residual field was 18 G. MRT casts courtesy NDT&CT.

5. Verification of Adequate Field Strength

The analyses presented in the previous section point to the importance of the ratio of M_0 to $|H_t|$ in the formation of residual-field MRT indications. Achieving an adequate permanent magnetisation M_0 of the test specimen is clearly critical to successful residual-field MRT. Given the range of inspection geometries and magnet configurations, verification of adequate magnetisation in residual-field MRT using longitudinal fields is not a trivial task.

Typically, when performing residual-field MRT using a longitudinal magnetising field, the presence of adequate field strength was verified by ensuring that H_t , the tangential component of the residual magnetic field as measured in air immediately above the region of interest, lies within a specified range. However, whilst confirmation that the measured tangential field lies in this range ensures that the component is in a remanent magnetic state, results such as those shown in Figure 5(b) where indications were reduced in length or even absent demonstrate that this requirement may not be sufficient to ensure the highest inspection sensitivity and reliability in all cases. Indeed, H_t is primarily a function of the strength and spatial arrangement of the magnetic pole – and depends as much on the magnet configuration and the component geometry as the internal specimen magnetisation at the measurement location (see Appendix A). Furthermore, in residual-field MRT, it is impossible to guarantee with any certainty the actual state of magnetisation within a component without full knowledge of the history of fields applied. For this reason, measurement of the tangential component of the field H_t alone does not uniquely determine the specimen magnetisation.

Hence, for residual-field MRT, rather than only specifying a required value for the residual tangential field arising from the remanent magnetisation, it is more important to specify the H_{max} value used to initially magnetise the specimen. According to Stanley [12], in a study of magnetic inspection techniques in the oil industry, H_{max} should be chosen to lie to the right of the peak in the rate of change of the remanent magnetic flux density B_r with H_{max} ,

$$\frac{1}{\mu_0} \frac{dB_r}{dH_{max}}. \quad (12)$$

The relationship between B_r and H_{max} for D6ac steel is shown in Figure 11 and is obtained from the series of hysteresis loops given previously [28]. The rate of change of B_r with H_{max} is plotted in Figure 12. The maximum rate of change is located at the value $H_{max} \approx 30$ Oe. If Stanley's requirement for MPI can be applied to MRT, it follows that H_{max} for residual-field MRT of D6ac must exceed 30 Oe. The evidence from CCMRT discussed in Section 7 suggests that the optimum value for H_{max} must 'lie to the right' of 30 Oe by a considerable amount, with a recommended value for H_{max} in the range 100 – 200 Oe. In this case the material is initially magnetised closer to saturation.

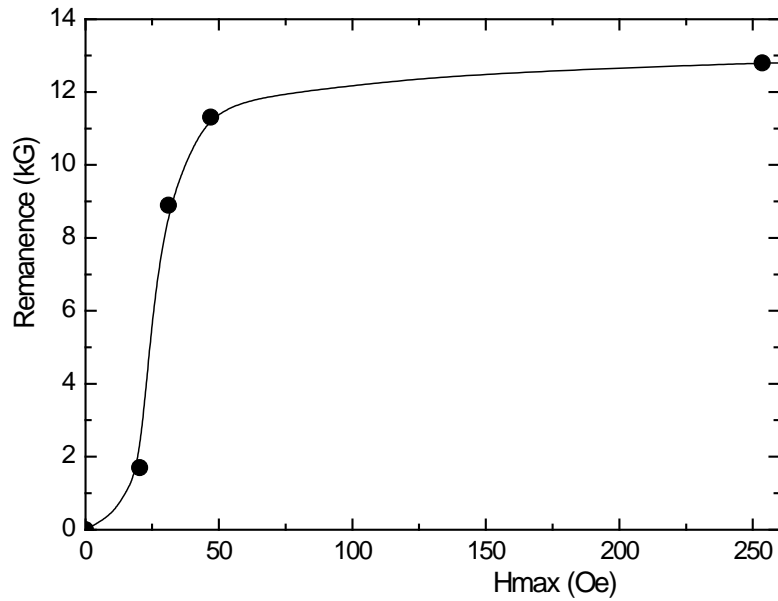


Figure 11 Variation of remanent magnetic flux density with the maximum applied magnetic field strength for D6ac steel (solid points). D6ac is effectively saturated after application of H_{max} of ~150 Oe. The solid curve is shown only as a guide to the eye.

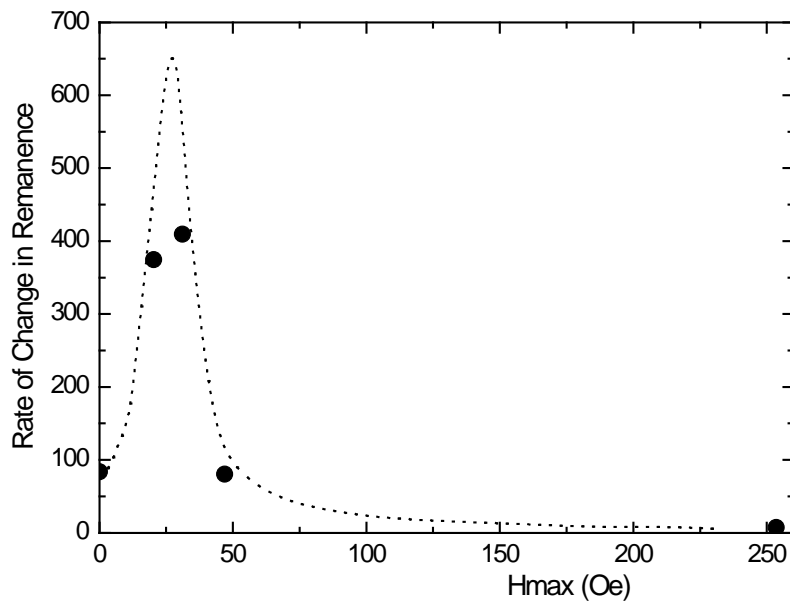


Figure 12 The rate of change in remanent magnetic flux density with maximum applied magnetic field strength (solid symbols) obtained from Figure 11 by numerical differentiation of the B-H data. The dotted curve shows the differential magnetic permeability as a function of applied field for comparison. The peak in the rate of change of remanence and the peak in the differential permeability occur at a similar magnetic field strength.

The meaning of adequate magnetisation for residual-field MRT can only be assessed relative to the smallest crack that needs to be reliably detected (a_{NDI}) for a particular inspection. It is clear that consistently adequate magnetisation cannot be universally guaranteed through a specification of the residual H_t at the specimen surface alone. Specification of both H_t and H_{max} would be an improvement, though even then it is unlikely that general design rules (similar to active-field MRT) to assure a specified a_{NDI} could be devised for residual-field MRT, because their performance will depend strongly on the actual specimen geometry and field configuration. Consequently, formulation of design rules which could be used with confidence for residual-field MRT across a wide range of specimen geometries would be very difficult.

The one clear exception to the difficulties with defining design rules for residual-field MRT is the special case of CCMRT, which relies on circular magnetisation. As discussed in Section 7, the simple geometry involved, combined with experimental data from POD trials has enabled the formulation of design rules based on minimum levels of applied H_{max} (expressed in terms of magnetising current as a function of hole diameter [29]) and maximum permitted levels of remanent field H measured around the hole subsequent to magnetisation.

The experience with active-field MRT and understanding of the fundamental principles underpinning residual-field MRT indicate that the technique should be relatively tolerant of moderate deviations from ideal conditions so that inadequate magnetisation is expected to result in a gradual degradation in performance and a gradual (rather than sudden) increase in a_{NDI} .

6. Finite-Element Modelling

The feasibility of using electromagnetic finite-element modelling (FEM) to support the development of MRT inspection procedures was also examined. In principle, FEM can be used to predict the magnetic field both inside and outside the material in the critical region to provide confidence that the magnetisation will be adequate for the inspection. Conformance with the modelled inspection conditions could then be established by comparing the predicted local normal and tangential components of H to those measured just above the surface of the component using a gaussmeter.

The major benefit of electromagnetic FEM is expected to be for residual-field MRT, as an accurate prediction of the residual magnetisation within a component, as well as the external demagnetising fields in the region of interest, would remove much of the uncertainty surrounding the technique.

In the past, FEM software developed in-house at Colorado State University was applied to modelling 2-D residual-field MFL from slots with varying degrees of success [11, 13, 15]. To the authors' knowledge, there are currently no commercial 3-D electromagnetic FEM codes available that can adequately predict the fields produced in practical residual-field MRT. It should also be noted that in order to model residual-field MRT, an accurate description of the entire B - H curve is essential.

More generally, a literature review did not reveal any alternative methods for successfully calculating 3-D residual magnetic fields in structural steels. In a 2006 review of residual magnetisation techniques applied to magnetic characterisation of structural steels, Sandomirskii [30] concluded that 'none of the [theoretical] attempts have enabled correct calculation and analysis of the distribution of residual induction [in steel] after pole magnetisation'. Babbar and Clapham [9] similarly conclude that 'finite element models cannot be used for this purpose unless domain level phenomena are incorporated into the model'.

It appears that substantial work will be required before off-the-shelf tools capable of modelling 3-D residual magnetisation effects for MRT of ferromagnetic steels become available.

7. Central-conductor Magnetic Rubber Testing

For completeness, this report concludes with a summary of improvements made to the design rules and practice of CCMRT for D6ac steel. These improvements were initiated from a parallel DSTO study into CCMRT inspection reliability [2, 24, 31]. For CCMRT, the test region is the inside bore and edges of holes. A circular magnetisation is provided by a conducting rod inserted through the hole to be inspected [4].

There are several reasons why the uncertainties discussed previously for residual-field MRT using longitudinal magnetising fields do not apply to the central-conductor variant of MRT, which relies on circular magnetisation.

- For CCMRT of D6ac steel, there is less scope for variations in the specimen geometry and magnetisation method compared with residual-field techniques using longitudinal magnetising fields. The only likely variations in CCMRT are those due to a non-circular hole shape, eccentric conductor placement [29], the proximity of any geometric features (such as edges) near the hole and possible eddy-current effects arising from the use of pulsed DC fields for magnetisation [32].
- For central-conductor geometries, the maximum applied field H_{\max} can be readily calculated (via the applied current) and controlled. This provides more confidence in achieving the required remanent magnetisation within the specimen.
- Complicating effects due to reversed tangential fields arising from magnetic poles are eliminated or at least minimised. For a conductor concentric in a circular hole in a large plate, the resultant magnetisation within the material is circumferential and axisymmetric so that the remanent magnetic field outside the specimen is zero ($H_t = H_n = 0$) in principle.

and, perhaps most importantly

- POD studies performed by DSTO have established the inspection reliability achieved in practice for CCMRT for D6ac aircraft components [2].

As part of POD trials, DSTO investigated the potential sources of unreliability in the CCMRT process. The most significant risk to successful CCMRT is the failure to adequately magnetise the hole. This could result from either (i) a deficiency within the defined process for a particular CCMRT inspection or (ii) operator omission whilst undertaking the inspection. These risks have been mitigated by (i) the development of specialised design rules for CCMRT and (ii) the use of magnetic flux indicators, as discussed below.

A series of design rules have been developed and implemented in order to specify the required DC current for CCMRT of D6ac steel. In line the POD trials, the recommended central-conductor current for magnetisation of circular holes to achieve $a_{\text{NDI}} = 0.51 \text{ mm}$ (0.020 inch) is 50 A/mm of hole diameter, so that a current of 500 A results in a calculated field $H_{\text{max}} = 200 \text{ Oe}$ at the surface of a 10 mm diameter hole. Lower values of current are permitted but with the acknowledgment that the inspection reliability is reduced. For example, it has been estimated that a_{NDI} increases to 0.91 mm (0.036 inch) if the current is reduced to 32 A/mm of hole diameter. This requirement is in line with the threading bar method used in the related technique of MPI [29], for which the accepted current is 28 A/mm. For MPI, the type of steel and expected reliability is not specified.

A simple software tool has been developed at DSTO to assist NDT procedure developers to design CCMRT inspections. An overview of this tool is given in Appendix B.

For CCMRT, in the absence of a defect, a correctly magnetised cast is practically indistinguishable from one for which no magnetic field was applied. Consequently, the use of a magnetic flux indicator (MFI) for all central-conductor magnetic rubber tests is recommended wherever technically feasible to alert the inspector that magnetisation of the hole had been omitted.

The MFI is a thin annulus of magnetic steel, painted on one side, containing a through-thickness electro-discharge machined slot on the outer diameter of the annulus, Figure 13(a) [2]. The MFI is constructed to have the same shape as the hole to be inspected but with a slightly larger inner diameter to permit inspection of the edges of the hole. A demagnetised MFI is taped to the surface of the test piece, with the painted face of the MFI in contact with the specimen throughout the inspection as shown in Figure 13(b). Once the current has been applied to the central-conductor and the inspection performed, the indication provided by the MFI provides a permanent record on the cured CCMRT cast that adequate magnetisation has been achieved around the hole. A cast showing the MFI response for adequate hole magnetisation is shown in Figure 14(a), where the MFI slot area is covered in magnetic particles and further particles have been drawn towards the slot tip. The resultant CCMRT cast from an elongated hole containing a fatigue crack is shown in Figure 14(b). The crack indication, in this case of length 2.3 mm (0.090 inch), is clearly visible in the rubber cast.

In circumstances where the axial symmetry has been lost (e.g. due to non-circular holes or the presence of edges), magnetic poles will be created on the specimen surface and give rise to a non-zero H_t and H_n . Thus, rather than being located on the vertical axis at $H = 0$ (point B_r in Figure 2), the magnetic operating point moves into the 2nd quadrant of the B - H

curve. To further define the boundaries for acceptable CCMRT inspection conditions, limitations can be placed on the magnitude of the reversed tangential field component and the normal field component arising in such cases where axial symmetry is lost. For example, it was proposed that the tangential field in the direction opposite to the magnetising field should not exceed 5 G in the region of interest, with no limit applied to the tangential field component in the same direction as the magnetising field. It is not possible to assess whether such a requirement is overly conservative without a parallel investigation into the impact on inspection reliability.

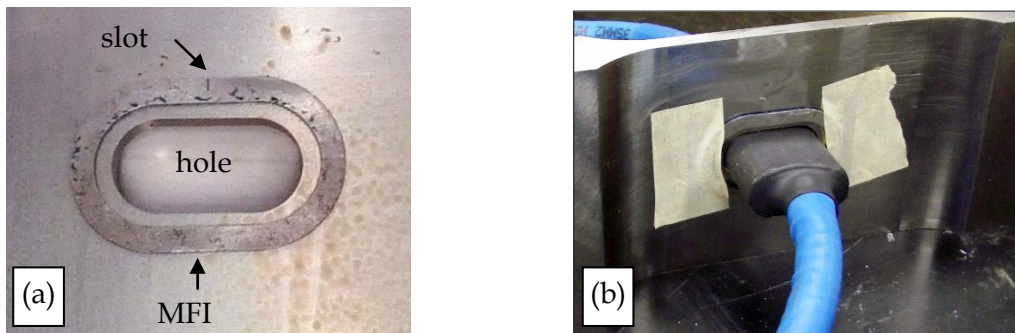


Figure 13 Typical CCMRT inspection arrangement using a MFI. (a) MFI located on the hole to be inspected. (b) Central-conductor passing through the MFI and hole prior to magnetisation and magnetic rubber pour. The dam for the magnetic rubber has not been constructed at this stage.

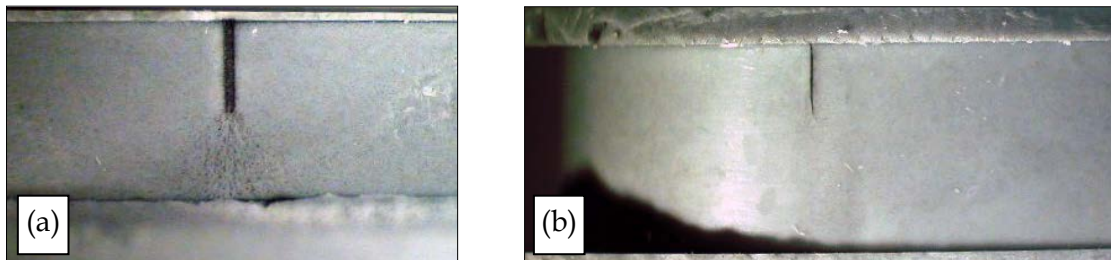


Figure 14 (a) Image of the MRT cast in the area of the MFI showing a concentration of magnetic particles covering the slot area and drawn towards the MFI slot tip. This demonstrates that the hole has been magnetised. (b) Cured CCMRT cast from the bore of the elongated hole in a D6ac steel test specimen. A 2.3 mm (0.090 inch) corner crack indication is visible along the position of the hole bore.

8. Future work

Residual-field MRT has certain practical advantages over active-field MRT but remains less well understood. Future enabling research, aimed at improved NDT capabilities using this niche technique for existing and future aircraft applications, would be useful.

Possible areas for future work include:

- Finite element modelling of residual magnetic fields in high-strength steel components together with experimental validation.
- Fundamental experimental studies to examine magnetic leakage fields and the formation of crack indications in residual-field MRT with longitudinal magnetising fields. Systematic investigations are required as a function of defect size, specimen geometry and maximum applied field strength. Confirmation of the proposed mechanism for formation of white bands is also required.
- Improvements to the residual-field CCMRT inspection technique via the mathematical analysis technique of image construction [29] to determine the effects on the active magnetic field when the hole is close to an edge, or the central-conductor is offset from the centre of the hole.
- Investigation of the role of time-varying magnetic fields (through the application of pulsed-currents) in CCMRT and the effect of eddy-current shielding of the interior of the specimen as well as multiple retracing of minor B - H loops for multiple pulses [32].

9. Conclusions

This report examined a series of key questions regarding residual-field MRT. The work was initiated by the observation that, under certain conditions, crack indications could be shorter or even absent when using residual-field MRT compared with active-field inspections.

The main conclusions are as follows:

- Despite the superficial similarities, a review of the scientific and technical literature revealed fundamental differences between active- and residual-field MRT due to the underlying magnetisation processes. It was also apparent that residual-field magnetic methods are less well understood than the corresponding active-field techniques, particularly in regard to MRT for detection of realistic defects such as closed fatigue cracks.
- Unlike active-field MRT, adequate magnetisation for residual-field MRT cannot be guaranteed through the specification of the tangential component of the residual magnetic field H_t at the specimen surface. An important improvement would be to specify both H_t and the required applied field H_{max} for a particular inspection. In addition, as a rule of thumb, the magnetisation method should ensure that any

induced magnetic poles are located well away from the region of interest. However, it is unlikely that a simple general set of design rules that would assure the probability of detection of cracks with a specified size a_{NDI} could be devised for residual-field MRT using longitudinal fields. The exception is for CCMRT, which employs a circular magnetisation in a tractable geometry and for which design rules have been developed to assist MRT procedure developers.

- In principle, electromagnetic FEM could be used to predict the magnetic field both inside and outside the material in the critical region to provide confidence that the magnetisation is adequate for the inspection. Unfortunately, it appears that substantial work is still required before off-the-shelf tools capable of modelling practical geometries for residual-field MRT of ferromagnetic steels become available.
- As with many areas in NDE, we conclude that the only robust way to establish experimentally whether the residual magnetisation is adequate for a given component and magnetisation geometry is through a POD trial.
- As mentioned above, it was reported that under certain conditions of magnetisation and specimen geometry, crack indications in residual-field MRT could be shorter or even absent apart from the presence of a faint white band. Simple model calculations of the forces acting on magnetic particles indicate that the presence of a reversed tangential field at the specimen surface, coupled with a weak leakage field due to inadequate magnetisation, is the likely mechanism behind this observation. The reason was not merely that the field was inadequate to produce crack indications but that the combination of reversed tangential fields and crack leakage fields appears to lead to a repulsion of magnetic particles from the crack location. To the authors' knowledge, this phenomenon has not been described previously.

Drawing these results together, the general conclusion is that active-field MRT is strongly preferred to residual-field MRT due to the current lack of design rules for residual-field MRT procedures which would assure the probability of detection of defects with sufficient confidence. The exception is central-conductor variant of residual-field MRT for which suitable design rules have been established which are supported by empirical POD trials.

This work and that in a companion report [1] have extended the scientific understanding of the magnetic rubber testing process and the available engineering data to underpin the application of MRT to aircraft. The improved understanding of MRT will also benefit related magnetic inspection methods, such as MPI of welded structures.

Acknowledgements

The authors wish to acknowledge the contributions from DSTO and RAAF personnel to this work over several years. In particular, we wish to thank the NDT procedure development staff at NDT&CT for their initial experimental work, valuable discussions and the provision of micrographs and other images related to this work. We also wish to thank Stephen Sanderson and Dr Tony Christopoulos for their insight and guidance on the state-of-the-art for electromagnetic FEM. The magnetic properties of D6ac steel were determined under contract by the National Measurements Institute, Lindfield. Finally, we wish to acknowledge the critical input provided by Dr Cayt Rowe (née Harding) in the genesis of the central-conductor field calculator and the development of the magnetic flux indicators.

References

- [1] Burke SK, Ibrahim ME, and Hugo GR (2014), *Principles and Application of Magnetic Rubber Testing for Crack Detection in High-Strength Steel Components: I. Active-Field Inspection*, Defence Science and Technology Organisation, DSTO-TR-3032, Melbourne, Australia.
- [2] Harding CA and Hugo GR (2007), *Probability of Detection for Central-Conductor Magnetic Rubber Testing*, Defence Science and Technology Organisation, DSTO-CR-2007-0206 Melbourne, Australia.
- [3] Weltman HJ, Carroll MT, Halkias JT, Kaarlela WT, and Reynolds JT (1975), 'Method and Composition for Detecting Flaws in Metallic Surfaces, Holes and Otherwise', US Patent 3862047, 1975.
- [4] Moore DG (2008), 'Magnetic Particle Testing' *Nondestructive Testing Handbook*; Vol. 8, 3rd ed., edited by Moore P (ASNT, New York).
- [5] Jiles D (1998), *Introduction to Magnetism and Magnetic Materials*, 2nd ed. (Chapman and Hall, London).
- [6] Jackson JD (1999), *Classical Electrodynamics*, 3rd ed. (Wiley, New York).
- [7] Cullity BD and Graham CD (2009), *Introduction to Magnetic Materials*, 2nd ed. (Wiley IEEE Press).
- [8] Weltman HJ, Carroll MT, Halkias JT, Kaarlela WT, and Reynolds JT (1978), 'Castable Magnetic Particle Flaw Detection Composition and Method Using Constituents That Are Non-Volatile and Resistant to Oxidation Below 100 F and Having a Viscosity Less Than 12000 Centipoises', US Patent 4121157, 1978.
- [9] Babbar V and Clapham L (2003), 'Residual Magnetic Flux Leakage: A Possible Tool for Studying Pipeline Defects', *Journal of Nondestructive Evaluation* **22** 117-125.
- [10] Schmidt JT and Skeie K (1989), 'Magnetic Particle Testing' *Nondestructive Testing Handbook*; Vol. 6, 2nd ed., edited by McIntyre P (ASNT, New York).
- [11] Lord W, Bridges JM, Yen W, and Palanisamy R (1978), 'Residual and Active Leakage Fields around Defects in Ferromagnetic Materials' in *ASNT Spring Conference*, New Orleans, LA, (ASNT).
- [12] Stanley RK (1985), 'Basic Principles of Magnetic Flux Leakage Inspection Systems for Evaluation of Oil Country Tubular Goods' in *Electromagnetic Methods of Non-*

- Destructive Testing*; Vol. 3, edited by Lord W (Gordon and Breach Science Publishers, London), p. 97.
- [13] Udpa SS, Sun YS, and Lord W (1988), 'Alternative Demagnetisation Curve Representations for the Finite Element Modelling of Residual Magnetism', *IEEE Transactions on Magnetics* **24** 226–229.
 - [14] Heath SE (1984), 'Magnetostatic Leakage Field Modelling', in *Review of Progress in Quantitative Nondestructive Evaluation*; Vol. 3, edited by D.E.Chimenti and D.O.Thompson (Plenum, New York, 1984), pp. 847–854.
 - [15] Heath SE (1984), 'Residual and Active Field Magnetostatic Modelling', M.Sc. Thesis, Department of Electrical Engineering, Colorado State University, Fort Collins, CO.
 - [16] Graham BC and Moore DG (2008), 'Magnetic Particle Sensitivity' in *Magnetic Particle Testing*; Vol. 8, 3rd ed., edited by Moore DG (ASNT, Columbus, OH), pp. 194–206.
 - [17] Förster F (1985), 'On the Way from the "Know-How" to the "Know-Why" in the Magnetic Leakage Field Method of Nondestructive Testing (Part Two)', *Materials Evaluation* **43** 1398–1404.
 - [18] Förster F (1985), 'On the Way from the "Know-How" to the "Know-Why" in the Magnetic Leakage Field Method of Nondestructive Testing (Part One)', *Materials Evaluation* **43** 1154–1162.
 - [19] Sponder L, Athinotis N, and Clark G (1992), 'Magnetic Leakage Field Ndi Development for Aerospace Components', *Non-Destructive Testing Australia* **29** 133–136.
 - [20] Beissner RE, Matzkanin GA, and Teller CM (1980), *Nde Applications of Magnetic Leakage Field Methods: A State-of-the-Art Survey*, NTIAC Southwest Research Institute, San Antonio, TX.
 - [21] Lord W and Srinivasan L (1984), 'Deconvolution of Defect Leakage Fields Obtained Using Hall Element Probes', in *Review of Progress in Quantitative Nondestructive Evaluation*; Vol. 3 (1984), pp. 855–862.
 - [22] Zagidulin RV (1998), 'Calculation of the Remanent Magnetic Field of a Continuity Defect in a Ferromagnetic Article. I. The Magnetic Field inside a Ferromagnetic Material', *Russian Journal of Nondestructive Testing* **34** 717–726.
 - [23] Zagidulin RV (1998), 'Calculation of the Remanent Magnetic Field of a Continuity Defect in a Ferromagnetic Article. Ii. The Remanent Magnetic Field of a Defect in Air', *Russian Journal of Nondestructive Testing* **34** 727–773.
 - [24] Harding CA and Hugo GR (2002), *Experimental Determination of the Probability of Detection for Magnetic Rubber Inspections of F-111 Steel Components*, Defence Science and Technology Organisation, DSTO-TN-0420, Melbourne, Australia.
 - [25] Burke SK and Ibrahim ME (2007), *Restrictions on the Ratio of Normal to Tangential Field Components in Magnetic Rubber Testing*, Defence Science and Technology Organisation, DSTO-TR-1991, Melbourne, Australia.
 - [26] Edwards C and Palmer SB (1986), 'The Magnetic Leakage Field of Surface-Breaking Cracks', *Journal of Physics D: Applied Physics* **19** 657–673.
 - [27] Bowler JR and Bowler N (2002), 'Evaluation of the Magnetic Field near a Crack with Application to Magnetic Particle Inspection', *Journal of Physics D: Applied Physics* **35** 2237–2242.

- [28] Burke SK and Ibrahim ME (2007), *Electrical and Magnetic Properties of D6ac Steel*, Defence Science and Technology Organisation, DSTO-TN-0757, Melbourne, Australia.
- [29] Edwards C and Palmer SB (1981), 'An Analysis of the Threading Bar Method of Magnetic Particle Flaw Inspection', *NDT International* 177-179.
- [30] Sandomirskii SG (2006), 'Application of Pole Magnetization in Magnetic Structural Analysis (Review)', *Defektoskopiya* **42** 586-609.
- [31] Harding CA and Hugo GR 'Probability of Detection for Magnetic Rubber Inspections of F-111 Steel Components' in *Proceedings 10th Asia-Pacific Conference on NDT APCNDT*, Brisbane.
- [32] Moake GL and Stanley RK (1985), 'Capacitor Discharge Magnetization of Oil Country Tubular Goods' in *Electromagnetic Methods of Non-Destructive Testing*; Vol. 3, edited by Lord W (Gordon and Breach Science Publishers, London), pp. 151-160.
- [33] Osborn JA (1945), 'Demagnetizing Factors of the General Ellipsoid', *Phys.Rev.* **67** 351-357.

This page is intentionally blank

Appendix A: Residual Magnetisation

A simplified model is presented to illustrate that measurement of H_t alone is not sufficient to determine the residual magnetic state for longitudinal magnetisation in MRT.

The idealised case examined consists of three ellipsoidal D6ac test specimens initially magnetised by applying and then removing a uniform field H_{\max} parallel to the long axis (for example using a cable-wrap solenoid). These specimens take the form of a long thin prolate ellipsoid of revolution with length-to-maximum-diameter ratios k of 8.86, 36.4 and 102 respectively. The ellipsoid having a ratio of 8.86 is depicted in Figure A1 where the highly idealised nature of the specimens is apparent. The prolate ellipsoid was chosen for this study because analytic solutions exist for this shape.

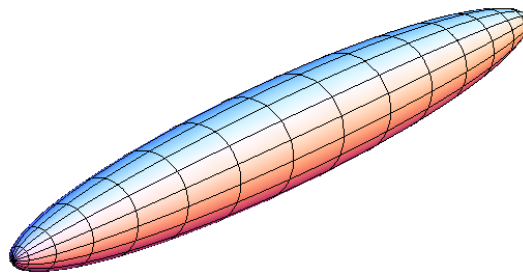


Figure A1 A prolate ellipsoid of revolution having a length-to-maximum-diameter ratio of 8.86.

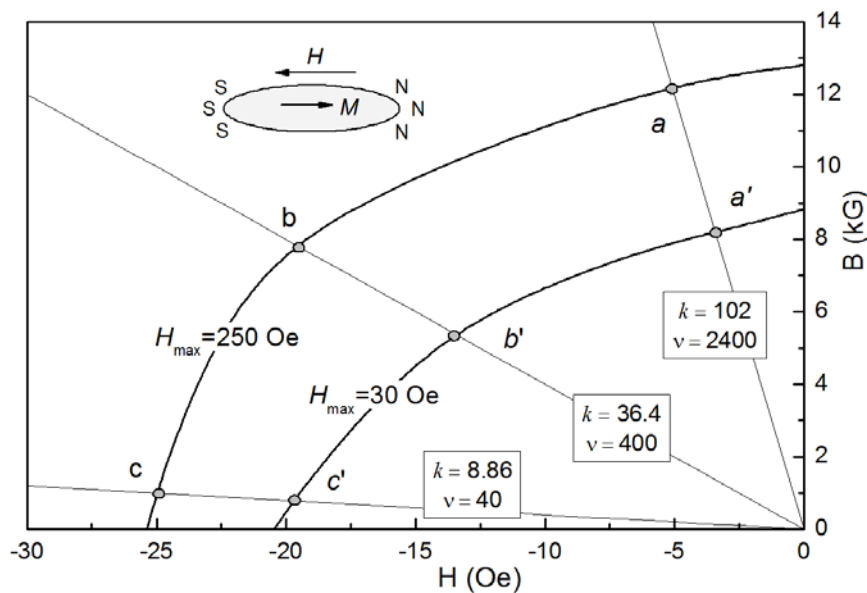


Figure A2 Operating points ($a - c$, $a' - c'$) for residual-field MRT illustrated using ellipsoidal D6ac specimens with aspect ratios k indicated. The B-H curves for D6ac steel after application of uniform fields $H_{\max} = 250$ Oe and $H_{\max} = 30$ Oe respectively (solid curves) are shown together with load lines (solid lines) for permeance values $v = 40$, 400 and 2400. The residual-field operating points (labelled) for a given specimen geometry are located at the intersection of the load lines and B-H curves.

Figure A2 shows the B - H curves (demagnetisation curves) after application of fields $H_{max} = 30$ Oe and $H_{max} = 250$ Oe together with the load lines for the three specimens.

The load or demagnetisation lines shown in Figure A2 are given by the expression [5]

$$B = -\mu_0 \nu H \quad (A1)$$

where μ_0 is the permeability of free space and ν is the permeance coefficient,

$$\nu = (1 - N_d) / N_d. \quad (A2)$$

N_d , the demagnetisation factor, is a function of the shape of the specimen. For a prolate ellipsoid [33],

$$N_d = \frac{1}{k^2 - 1} \left[\frac{k}{\sqrt{k^2 - 1}} \ln(k + \sqrt{k^2 - 1}) - 1 \right], \quad (A3)$$

where k is the length-to-diameter ratio for the ellipsoid.* The load lines in Figure A2 correspond to permeance values of $\nu = 40$, 400 and 2400, and were calculated using Eq. (A1) for the specimen k values of 8.86, 36.4 and 102 respectively.

According to magnetic theory, the values of B and H within the specimen are uniquely determined by the intersection of the load line and the demagnetisation curves. These operating points are shown in Figure A2 and are denoted by the points a , b , c for specimens magnetised using the higher field $H_{max} = 250$ Oe and by a' , b' , c' for specimens magnetised using the lower field $H_{max} = 30$ Oe.

The relevant features illustrated by Figure A2 for residual-field MRT are as follows:

- In this simple example where the specimen is uniformly magnetised, the state of magnetisation in the material is uniquely specified by measurements of both H_{max} and H_t . Measurements of either one of these parameters is insufficient. For example, while the operating points b and c' both correspond to the same value of $H_t \approx -20$ Oe measured using a gaussmeter (device for measuring magnetic flux) in practical MRT, the magnetic flux density B within the material for the two specimens differs by almost an order of magnitude from ~ 0.8 kG (c') to ~ 8 kG (b).
- The resulting flux density in the test specimen depends on the specimen geometry (k) as well as H_{max} . In the case shown in Figure A2, the highest magnetic flux density in the material (operating point a) is achieved for the needle-like specimen ($k = 102$, $\nu = 2400$) magnetised using $H_{max} = 250$ Oe. A lower flux density (operating point b) is obtained for the specimen with intermediate k ($k = 36.4$, $\nu = 400$) magnetised using the same H_{max} and lower value still (operating point c) for the specimen with the smallest k ($k = 8.86$, $\nu = 40$).

* The derivation of these relationships is presented in intermediate text books on electromagnetism, see for example Jiles [5]

- A high value of H_{max} combined with an unfavourable geometry can produce a similar magnetisation to that of a favourable geometry and low H_{max} . In this way, the flux density in the material for the specimen with intermediate k ($k = 36.4$) magnetised using $H_{max} = 250$ Oe (operating point b) is similar to that of the specimen with the largest k ($k = 102$) magnetised using the lower $H_{max} = 30$ Oe (operating point a').

In summary, the resultant magnetisation depends on the magnetic properties of the material (B - H curves), the specimen geometry (ellipsoid, aspect ratio k), the field configuration (uniform field applied parallel to the long axis) as well as H_{max} . Measurement of H_t alone is not sufficient to determine the residual magnetic state.

In practical MRT, the applied fields and the resultant remanent magnetisation are 3-D and non-uniform so significantly more complicated than the simple model calculations leading to the results in Figure A2. Nevertheless, the same general principles apply. For example, one may expect that a high magnetisation would be achieved for the configuration shown in Figure 5(a) because H_{max} is likely to be large and the field is applied in such a way that the effective permeance would also be large. In the case shown in Figure 5(b), the magnetisation is expected to be weaker, as H_{max} is likely to be smaller due to the awkward configuration of the electromagnet pole pieces.

Appendix B: Central-conductor Field Calculator

This appendix contains a description of the simple Microsoft Excel® software tool developed by DSTO for determination of CCMRT test parameters in order to ensure adequate magnetisation of components.

Figure B1 shows a worksheet which can be used to determine of the magnetic field (in Gauss) at the surface of a test component bolthole in which a cylindrical conductor carrying a DC current has been symmetrically inserted. The field is determined using the Biot-Savart law reduced to the case of a long, straight wire of circular cross-section.

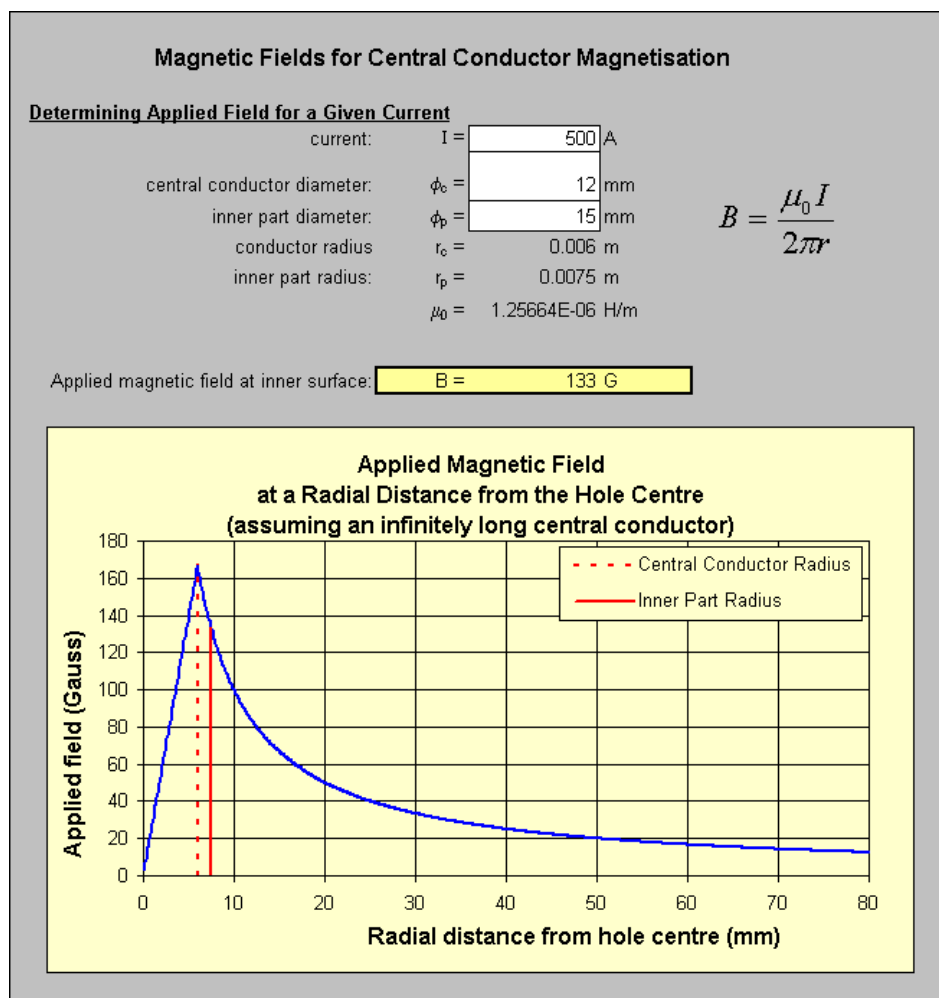


Figure B1 Calculation of the magnetic field applied to a component via a current-carrying central conductor inserted symmetrically within a bolthole, using the Biot-Savart law for a current-carrying wire.

Figure B2 shows the calculator worksheet which can be used to determine the required current within the conductor in order to achieve an $a_{NDI} = 0.51$ mm (0.020 inch) for the inspection, benchmarked from previous DSTO/RAAF POD trials. The calculator also includes a recommended minimum central-conductor length, determined in order to provide a maximum range of magnetic field values in the region of interest of $\pm 11\%$ about the mean value, and a correction for finite conductor length again using Biot-Savart for a U-shaped wire. The value of $\pm 11\%$ corresponds to ± 25 G about a mean value of 200 G.

(a) **Determining Required Current for a Given Geometry**

Part Geometry

inner part diameter: $\phi_1 =$ mm
 inner radius: $r_1 =$ 0.0075 m
 $\mu_0 =$ 1.3E-06 H/m

To achieve $a_{NDI} = 0.020$ "

Applied magnetic field at inner surface: $B =$ 133 G
 required current: $I_{(a_{NDI} = 0.020") =}$ **498.75 A**

(b) **Recommended Minimum Central Conductor Length**

inner part diameter: $\phi_1 =$ 15 mm (from above)
 thickness of component (length of hole): $t =$ mm

minimum total length of central conductor: **136 mm**
 minimum length protruding from each end of hole: **63 mm**

(c) **Correction for Finite Conductor Length**

current: $I =$ 500 A
 inner part diameter: $\phi_p =$ 15 mm
 central conductor length: mm
 thickness of component (length of hole): $t =$ mm

Magnetic field variation

A =	121 G
B =	147 G
C =	121 G
D =	147 G

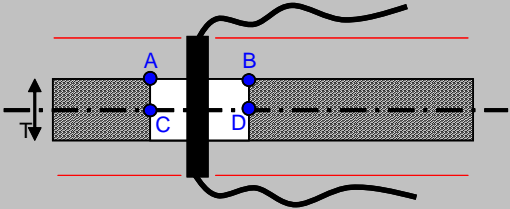


Figure B2 Central-conductor software tool for the calculation of (a) the current required for a component (bolthole) of given geometry, (b) the minimum length of conductor for a given part thickness, and (c) a correction using the Biot-Savart law to allow for the finite length of the central conductor.

The calculations above are combined into a single summary worksheet for use by NDT procedure developers, shown Figure B3. A linear interpolation is used to estimate a_{NDI} between the endpoints of 0.5 mm (0.020 inch) and 0.91 mm (0.036 inch) for which POD data were available.

CENTRAL CONDUCTOR CALCULATOR

Determine Current Required for a Given Geometry

Part diameter
Part thickness, T

15

 mm

10

 mm

Recommend minimum length of central conductor =
 Recommended minimum length protruding from each end of hole =

136 mm

63 mm

Central conductor length

150

 mm

Note:
Central conductor length either protrudes equally from both ends of the hole or is calculated as twice the shortest protruding length + part thickness (mm)

a_{NDI}	Required Current
0.020	= 750 A
0.021	= 733 A
0.022	= 717 A
0.023	= 700 A
0.024	= 684 A
0.025	= 667 A
0.026	= 651 A
0.027	= 634 A
0.028	= 618 A
0.029	= 601 A
0.030	= 585 A
0.031	= 568 A
0.032	= 552 A
0.033	= 535 A
0.034	= 519 A
0.035	= 502 A
0.036	= 486 A

Figure B3 Central conductor field calculator front-end

DEFENCE SCIENCE AND TECHNOLOGY ORGANISATION DOCUMENT CONTROL DATA					
				1. PRIVACY MARKING/CAVEAT (OF DOCUMENT)	
2. TITLE Principles and Application of Magnetic Rubber Testing for Crack Detection in High-Strength Steel Components: II. Residual-Field Inspection			3. SECURITY CLASSIFICATION (FOR UNCLASSIFIED REPORTS THAT ARE LIMITED RELEASE USE (L) NEXT TO DOCUMENT CLASSIFICATION) <div style="display: flex; justify-content: space-between;"> Document (U) </div> <div style="display: flex; justify-content: space-between;"> Title (U) </div> <div style="display: flex; justify-content: space-between;"> Abstract (U) </div>		
4. AUTHOR(S) S K Burke, M E Ibrahim and G R Hugo			5. CORPORATE AUTHOR Defence Science and Technology Organisation 506 Lorimer St Fishermans Bend Victoria 3207 Australia		
6a. DSTO NUMBER DSTO-TR-3033		6b. AR NUMBER AR-016-113		7. DOCUMENT DATE December 2014	
8. FILE NUMBER 2009/1079036/1		9. TASK NUMBER AIR 07/101		10. TASK SPONSOR DGTA-ADF	
				11. NO. OF PAGES 33	
				12. NO. OF REFERENCES 33	
13. DSTO Publications Repository http://dspace.dsto.defence.gov.au/dspace/			14. RELEASE AUTHORITY Chief, Maritime Division		
15. SECONDARY RELEASE STATEMENT OF THIS DOCUMENT <div style="text-align: center;"><i>Approved for public release</i></div>					
OVERSEAS ENQUIRIES OUTSIDE STATED LIMITATIONS SHOULD BE REFERRED THROUGH DOCUMENT EXCHANGE, PO BOX 1500, EDINBURGH, SA 5111					
16. DELIBERATE ANNOUNCEMENT No Limitations					
17. CITATION IN OTHER DOCUMENTS Yes					
18. DSTO RESEARCH LIBRARY THESAURUS http://web-vic.dsto.defence.gov.au/workareas/library/resources/dsto_thesaurus.shtml magnetic rubber testing, measurement, magnetic fields, fatigue cracks, detection, steel, F-111 aircraft					
19. ABSTRACT Since its introduction in the 1970s, magnetic rubber testing (MRT) has been used successfully to inspect critical high-strength steel aerospace components for surface-breaking fatigue cracks. In the residual-field variant of MRT, inspections are performed following the application and subsequent removal of a magnetic field, relying on the remanent magnetisation of the component to produce crack indications. For certain geometries, residual-field MRT is capable of reliable detection of cracks as small as 0.43 mm (0.017 inch) in surface length. However, for other conditions of specimen geometry and magnet configuration, it was observed that crack indications could be shorter or even absent when using residual-field MRT compared with active-field inspections. This report presents the results of an experimental and theoretical study into the formation of residual-field MRT indications and the rationale for verification of adequate field strength. It is proposed that a combination of inadequate magnetisation, shallow crack depth and the presence of a reversed tangential magnetic field at the surface of the specimen contribute to these observed anomalies in residual-field MRT compared with active-field MRT. The results of a related investigation into active-field MRT are presented in a companion report.					